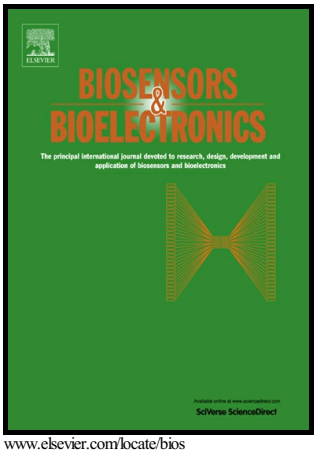

www.elsevier.com/locate/bios

Target-catalyzed hairpin assembly and metal-organic frameworks mediated nonenzymatic co-reaction for multiple signal amplification detection of miR-122 in human serum

Yuliang Li, Chao Yu, Bo Yang, Zhirui Liu, Peiyuan Xia, Qian Wang

PII: S0956-5663(17)30776-5
DOI: https://doi.org/10.1016/j.bios.2017.11.047
Reference: BIOS10123

To appear in: *Biosensors and Bioelectronic*

Received date: 13 September 2017
Revised date: 23 October 2017
Accepted date: 14 November 2017

Cite this article as: Yuliang Li, Chao Yu, Bo Yang, Zhirui Liu, Peiyuan Xia and Qian Wang, Target-catalyzed hairpin assembly and metal-organic frameworks mediated nonenzymatic co-reaction for multiple signal amplification detection of miR-122 in human serum, *Biosensors and Bioelectronic,* https://doi.org/10.1016/j.bios.2017.11.047

Target-catalyzed hairpin assembly and metal-organic frameworks mediated nonenzymatic co-reaction for multiple signal amplification detection of miR-122 in human serum

Yuliang Li[1], Chao Yu[2], Bo Yang[1], Zhirui Liu[1], Peiyuan Xia[1]*, Qian Wang[1]*

1 Department of Pharmacy, Southwest Hospital, Third Military Medical University, Chongqing 400038, P. R.China

2 Institute of Life Science and Department of Pharmacy, Chongqing Medical University, Chongqing 400016, P. R. China

*Corresponding author: Prof. Qian Wang and Peiyuan Xia,

Email: xqwq411@126.com (Q. Wang); py_xia2013@163.com (P.Y. Xia)

Tel: (86) 23-68754463

Full address: Department of Pharmacy, Southwest Hospital, Third Military Medical University, No.30 Gaotanyan Street, Shapingba District, Chongqing 400038, P. R. China.

ABSTRACT

Herein, a new type of multifunctional iron based metal-organic frameworks (PdNPs@Fe-MOFs) has been synthesized by assembly palladium nanoparticles on the surface of Fe-MIL-88NH_2 MOFs microcrystals, and first applied in electrochemical biosensor for ultrasensitive detection of microRNA-122 (miR-122, a biomarker of drug-induced liver injury). The nanohybrids have not only been utilized as ideal nanocarriers for immobilization of signal probes, but also used as redox probes and electrocatalysts. In this biosensor, two hairpin probes were designed as capture probes and signal probes, respectively. The nanohybrids conjugated with streptavidin and biotinylated signal probes were used as the tracer labels, target miR-122 was sandwiched between the tracer labels and thiol-terminated capture probes inserted in MCH monolayer on the gold nanoparticles-functionalized nitrogen-doped graphene sheets (AuNPs@N-G) modified electrode. Based on target-catalyzed hairpin assembly, target miR-122 could trigger the hybridization of capture probes and signal probes to further be released to initiate the next reaction process resulted in numerous tracer indicators anchored onto the sensing interfaces. Thus, the detection signal could be dramatically enhanced towards the electrocatalytic oxidation of 3,3',5,5'-tetramethylbenzidine in the presence of H_2O_2 owing to the intrinsic and intriguing peroxidase-like activity of the nanohybrids. With the assist of target-catalyzed hairpin assembly and PdNPs@Fe-MOFs mimetic co-reaction for signal amplification, a wide detection range from 0.01 fM to 10 pM was achieved with a low detection limit of 0.003 fM (S/N=3). Furthermore, the proposed biosensor exhibited excellent specificity and recovery in spiked serum samples, and was successfully used for detecting miR-122 in real biological samples, which provided a rapid and efficient method for detecting drug-induced liver injury at an early stage.

Keywords

Target-catalyzed hairpin assembly, metal-organic frameworks, drug-induced liver injury, microRNA-122, multiple signal amplification

1. Introduction

Drug-induced liver injury (DILI) is a major safety concern of clinical medicine and a common cause of drug failure or withdrawal during pharmaceutical industry (Larrey and Pageaux 2005). In western clinical medicine, nearly half of the cases of acute liver failure were caused by DILI (Fontana et al. 2014). If no effective treatments were given within a few hours of the occurrence of disease, liver transplantation may be the only therapeutic option for later presentation (Fontana et al. 2014). Recently, circulating microRNA-122 (miR-122) was regarded as a promising serum biomarker for the noninvasive diagnosis of liver injury at early stage (Antoine et al. 2013; Starkey Lewis et al. 2011). Thus, rapid and accurate detection of miR-122 is of great significance for the early diagnosis and timely treatment of liver injury.

At present, various analytical methods for the identification and quantification of microRNAs have been reported, such as northern blot (Valoczi et al. 2004), real-time quantitative polymerase chain reaction (qRT-PCR) (Yu et al. 2013) or microarray (Thomson et al. 2004), *et al*. Although these methods are widely used, some disadvantages still exist, such as long assay times, low detection accuracy, complex operation processes and stringent laboratory conditions, which cannot meet the need of fast and accurate diagnosis. Thus, a more accurate, simple and reliable diagnosis method is urgently needed. Among various analytical methods, the electrochemical sensors have received significant attention owing to their quick response, low cost, simple preparation and extensive applications in different fields (Su et al. 2017). Unfortunately, microRNAs analysis of electrochemical sensors still remain quite a challenge in accuracy and sensitivity because of the small size (18-25 nt) and the low abundance in biological samples. In order to overcome these challenges, many efforts should be devoted to the sensing platform and/or signal amplification strategies.

Nitrogen-doped graphene (N-G) sheets are a new single-atom-thick carbon material, and retain the intriguing characteristics of graphene, such as large surface area and good electrical conductivity (Chen et al. 2016). A large number of nitrogen atoms introduced to N-G sheets could create more defect sites and effectively avoid

the aggregation of above N-G sheets on the electrode surface. These defect sites could increase the biocompatibility of microenvironment, and make it easy to functionalize with metal nanoparticles (such as Au, Pd, and Pb nanoparticles). As previously reported (Chen et al. 2016), N-G sheets decoration with Au nanoparticles (Au/N-G) could load more capture probes (CPs) through strong Au-S bonds due to its large surface area and plentiful active sites, and also extensively improve the electron transfer between the biomolecules and electrode surface. Thus, Au/N-G was regarded as a promising supporting material. In addition to the number of CPs, the orientation and spatial distribution of the immobilized CPs on the electrode surface also played a vital role in the nucleic acid hybridization events, which impacted the sensitivity, selectivity and reproducibility of electrochemical biosensors (Josephs and Ye 2013; Mishra et al. 2014).

To further increase the sensitivity and selectivity of biosensors, enzyme-assisted or enzyme-free amplification strategies were commonly employed in the fabrication of electrochemical biosensors. Enzyme-assisted amplification included enzyme catalyzed reaction (Xia et al. 2015) and enzyme-assisted nucleic acid amplification technologies such as rolling circle amplification (Liu et al. 2014), strand displacement amplification (Wang et al. 2013) and nuclease-assisted hairpin assembly (Zhang et al. 2014), *et al*. However, these methods involved multiple operation steps and additional exogenous reagents and enzymes, and undoubtedly increased the experimental complexity, detection times and costs. Moreover, these biosensors were susceptible to environments because enzymes were easy to degenerate, inactivate and aggregate after they immobilized on the electrode surface so that certainly limited their applications. To overcome these disadvantages, researchers made efforts to construct many enzyme-free amplification methods, for instance, artificial enzyme mimetic as a substitute for enzyme-dependent reactions (Huang et al. 2014; Sun et al. 2013), hybridization chain reaction (Liu et al. 2013) and target-catalyzed hairpin assembly (TCHA) (Shuai et al. 2016; Yu et al. 2016). Iron based metal-organic frameworks (MOFs) have emerged as a new kind of crystalline materials because of their fascinating structures with huge surface area, excellent stability and intrinsic

peroxidase-like activity (Wang et al. 2016; Xie et al. 2015). Liu *et al.* used amino-containing MOFs host matrix to anchor gold nanoparticles adsorbing single-stranded DNA for preparing peroxidase mimic catalysts and applied the functionalized MOFs for colorimetric detection of DNA (Liu et al. 2015). Jiang *et al.* utilized MOFs matrix to assemble silver nanoparticles as SERS substrates and peroxidase mimic catalysts and applied the as-prepared MOFs for SERS detection of dopamine (Jiang et al. 2015). Up to now, most of the researches have focused on the peroxidase activity of functionalized MOFs for the colorimetric as well as SERS detection of the targets. To the best of our knowledge, there are no reports that MOF-based materials have been used in the construction of sandwich electrochemical sensor.

Inspiringly, TCHA has attracted extensive attention in recent years, for the signal amplification is easily achieved by the cycling use of the target (Yu et al. 2016). In this strategy, two hairpin probes were rationally synthesized to co-exist stably in solution. Firstly, the target opened and hybridized with one of hairpins (H_1) when the target microRNA was added. Then, another hairpin (H_2) was opened and hybridized with the previous opened hairpin and liberated target for the next cycle. Finally, each target can open and hybridize with a large amount of H_1, resulting in significant H_2 being captured. Consequently, our motivation is to adequately utilize the own peroxidase activity of functionalized MOFs and target-catalyzed hairpin assembly to obtain a new sandwich-type electrochemical biosensor for the detection of miR-122.

In this work, a relatively simple, enzyme-free and ultrasensitive electrochemical biosensor was constructed based on the ingenious combination of target-catalyzed hairpin assembly and nonenzymatic co-reaction for multiple signal amplifications. First, new nanohybrids (PdNPs@Fe-MOFs) of iron based metal-organic frameworks functionalized with palladium nanoparticles through electrostatic self-assembly using a cationic polymer, polyethyleneimine (PEI), as cross linker were designed and synthesized in this work for the first time. Second, the nanohybrids were utilized as nanocarriers due to large surface area and numerous active sites for the immobilization of biotin-labeled signal probes (H_2), and as tracer indicators to quickly

catalyze the oxidation of 3,3',5,5'-tetramethylbenzidine in the presence of H_2O_2. Third, target miR-122 was sandwiched between the tracers and thiol-terminated capture probes (H_1) inserted in MCH monolayer on the gold nanoparticles-functionalized nitrogen-doped graphene sheets (AuNPs@N-G) modified electrode. Finally, with the help of target-catalyzed hairpin assembly, target miR-122 could trigger the hybridization of H_1 and H_2 to further be released to initiate the next reaction process resulting in numerous tracer indicators anchored onto the sensing interfaces and a significant signal response as shown in Scheme 1D, which further improved the sensitivity of the biosensor. The stepwise fabrication process and signal amplification mechanism were illustrated in Scheme 1, which were described in detail in the experimental section.

2. Experimental

The "Chemicals and materials", "Apparatus and characterization" and "Preparation of AuNPs@N-G nanocomposites" are described in Supplementary Material.

2.1 Preparation of PdNPs@Fe-MOFs microcrystals

First of all, Fe-MIL-88NH_2 MOFs was synthesized according to the previous report of our group (Chen et al. 2017). Briefly, 0.187 g of iron (III) chloride hexahydrate ($FeCl_3 \cdot 6H_2O$) and 0.126 g of 2-aminoterephthalic acid were dissolved in 15 mL of DMF, and then 3.45 mmol acetic acid was added into this mixed solution. The mixture was placed in a silicone oil bath at 120 ºC for 4 h to crystallize. After cooling to room temperature, the nanoparticles were isolated by centrifugation and washed with DMF, ethanol and deionized water to remove the excess reactants, respectively. Finally, the resultant Fe-MIL-88NH_2 MOFs composites were dried in a vacuum oven.

PdNPs were prepared by reduction of Na_2PdCl_4 with sodium borohydride, and the reaction processes were similar to that of AuNPs (Li et al. 2015b). For the preparation of PdNPs@Fe-MOFs microcrystals, 200 μL PEI solution was slowly injected into 5 mL Fe-MIL-88NH_2 MOFs solution (1 mg mL^{-1}) by the weight ratio of PEI : Fe-MIL-88NH_2 MOFs to 4 : 1 under vigorously stirring and stirred for 12 h. Then, 200 μL of the prepared PdNPs colloid solution was added, and stirred for another 12 h. Finally, the resultant nanohybrids were centrifuged and washed with deionized water and ethanol for several times, respectively.

2.2 Preparation of PdNPs@Fe-MOFs/SA/SPs bioconjugates

The synthesis procedures were conducted in the following manner. In brief, 2 mg streptavidin was added dropwise into 2 mL PdNPs@Fe-MOFs nanohybrids (1 mg mL^{-1}) with gently stirring for 12 h at 4 ºC to make the streptavidin sufficiently anchored onto the surface of the nanohybrids. Then, 100 μL of biotinylated signal probes 1 (or signal probes 2) were injected and stirred for another 1 h to form the bioconjugates via the specific recognition between streptavidin and biotin. Finally, 1 mg BSA was added into the solution to block the non-specific binding sites. After centrifugation and washing, the tracer indicators 1 (or tracer indicators 2) were resuspended in 0.1 M PBS (pH 7.4) and stored at 4 ºC for the following experiments.

2.3 Preparation of the biosensor

Prior to use, the disulfide bonds of CPs were reduced by TCEP for 2 h at room temperature in the dark. Successively, the oligonucleotides were denatured at 95 ºC for 5 min and slowly cooled down to form the stem-loop structures. Before modification, the glassy carbon electrode (GCE) was pretreated with piranha solution (30% H_2O_2 / 98% H_2SO_4 = 1:3, v/v) for 20 min. After rinsing adequately with deionized water, the GCE was carefully polished to a mirror-like surface with 300 nm and 50 nm alumina powder sequentially, and followed successive sonication in ethanol and deionized water for 3 min. Then, it was further electrochemically cleaned

and activated in a H_2SO_4 solution (0.5 M) with the potential scanning from -0.35 to +1.6 V at a scan rate of 0.1 V s^{-1} until a reproducible cyclic voltammogram was required, and followed by rinsing with deionized water and drying in the air.

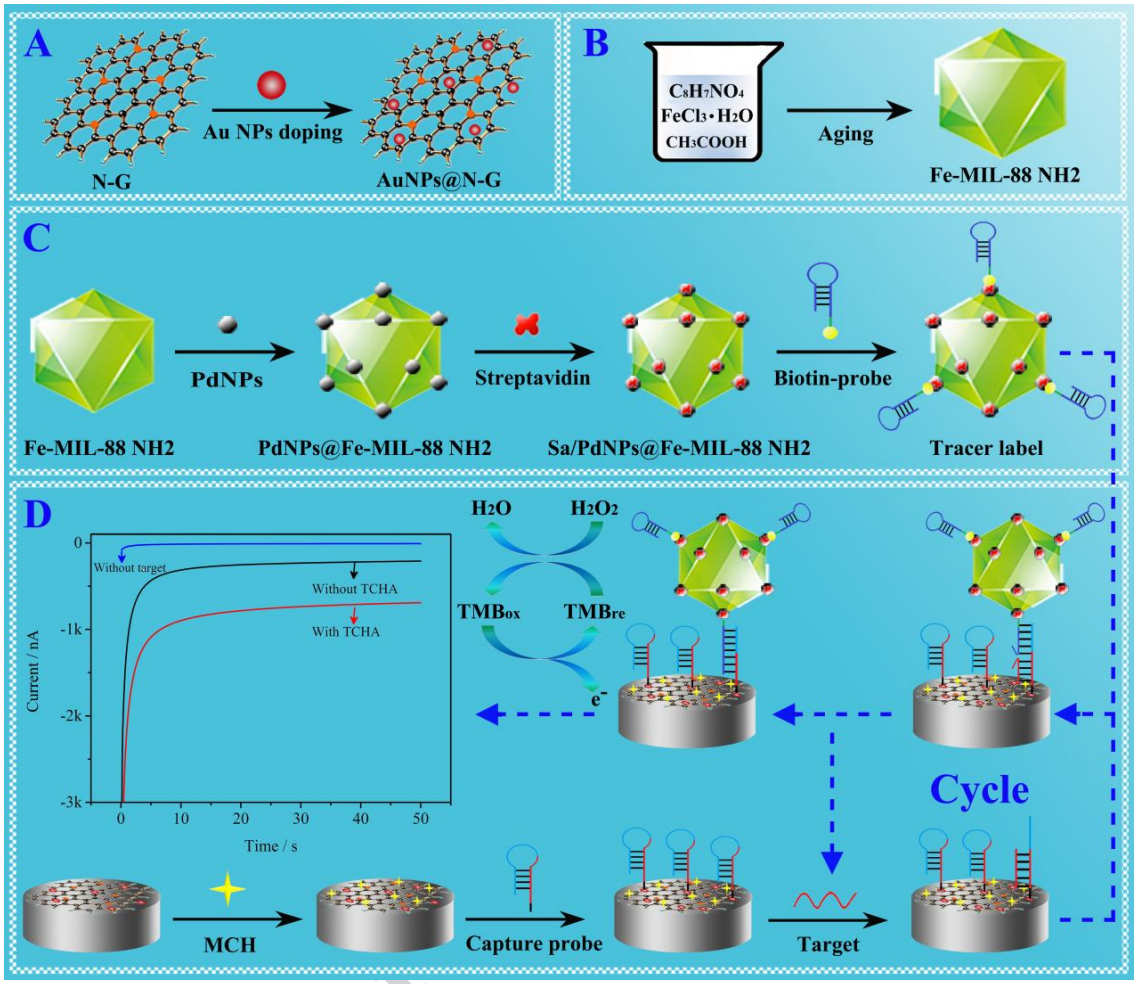

Scheme 1. Illustration of the electrochemical biosensor. The preparation process of AuNPs@N-G (A), Fe-MIL-88NH_2 MOFs (B), PdNPs@Fe-MOFs/SA/SPs bioconjugates (C) and the fabrication process of the biosensor and the target-catalyzed hairpin assembly for target recycle (D).

Afterwards, 10 μL AuNPs@N-G was cast onto the pretreated electrode and dried under an infrared lamp to form a uniform sensing film. Then, the electrode surface was blocked with 0.5 mM MCH for 15 min. After rinsing thoroughly with ddH_2O, the modified electrode was incubated with 10 μL of 2 μM CPs in the MCH matrix for another 30 min at room temperature. Then, an optimal CPs orientation was obtained by self-assembly on the surface of the electrode via Au-S bonds. Subsequently, the

as-prepared electrode was immersed in a mixture of 10 μL miR-122 standard solutions at various concentrations and 10 μL of the tracer bioconjugates, and incubated for 75 min at 45 ºC. To remove the physically adsorptive species, the obtained electrode was carefully washed with ddH_2O step by step. Finally, the fabricated biosensor was investigated in 0.1 M PBS (pH 4.0) containing 1 mM TMB and 20 μM H_2O_2 with the potential of 150 mV at room temperature (Sun et al. 2013; Wu et al. 2017). The electrochemical response signal was collected from the TMB-H_2O_2 catalysis reaction mediated by PdNPs@Fe-MOFs mimicking peroxidase, which gave the quantitative criteria for the electrochemical detection of miR-122.

3. Results and discussion

3.1 Characterization of the N-G and AuNPs@N-G nanohybrids

The structural features of the N-G and AuNPs@N-G nanocomposites were characterized by ultraviolet visible absorption spectra (UV-vis). As shown in Fig. S1A (see the Supplementary Material), the N-G (curve a) possessed a sharp absorption peak at 230 nm resulted from the characteristic of π→π* transition for C=C, and a shoulder absorption peak at 270 nm ascribed to the n→π* transition for C=O, which were highly similar to the performance of the graphene oxide sheets (Huang et al. 2010; Paredes et al. 2008). After decoration with Au nanoparticles on the surface or inner of N-G sheets, the tiny red shift in π→π* transition from 230 nm to 235 nm was observed, the shoulder absorption peak at 270 nm disappeared and a new and broad absorption band emerged at 560 nm (curve b), which could be attributed to the surface plasmon resonance characteristics of Au nanoparticles (Orendorff et al. 2006). Meanwhile, in order to confirm the synthesis processes and the chargeability, zeta-potential measurements were investigated before and after the modification of AuNPs and PEI on the N-G sheets, respectively. The average potential of the pure N-G sheets solution (Fig. S1B) showed a negative value at -17.1 mV, which could be assigned to that transformation of -COOH to COO^- (Yu et al. 2016). When

functionalized with PEI, the zeta-potential showed a positive value at +15.0 mV, which could be attributed to the transformation of COO^- to NH^+. The positive charges of PEI@N-G nanohybrids were beneficial for the absorption of $AuCl_4^-$ through electrostatic interaction, and then decorating negatively charged Au nanoparticles by the citrate reduction. After assembling AuNPs to PEI@N-G mixture solution, the zeta-potential was decreased to +8.4 mV, suggesting that a number of AuNPs were indeed assembled on the surface of the N-G sheets. All the above results indicated that the AuNPs@N-G nanohybrids had been successfully synthesized without the destruction of the N-G sheets structures.

The morphologies of the as-synthesized nanomaterial were characterized by SEM, TEM and FESEM, respectively. As shown in Fig. 1A and 1C, a thin layer of the N-G hybrids was presented with a typical crumpled and wrinkled structure, suggesting that the N-G hybrids were well maintained the two-dimensional morphology and the large surface area. After the reduction of $HAuCl_4$, numerous Au nanoparticles were in situ assembled and grown on the surface of the N-G sheets with an average diameter of 20 nm (Fig. 1B and 1D). Afterwards, the morphology and elemental compositions of the AuNPs@N-G nanocomposites were further investigated by the FESEM and EDS. A typical graphene-like structure and inhomogeneous Au nanoparticles attached outside the surface of the N-G were exhibited (Fig. 1E), both of which were in good agreement of the above SEM and TEM results. In addition, signature C, N and Au peaks were characterized by EDS (Fig. 1F), indicating that the AuNPs@N-G nanohybrids had been successfully synthesized.

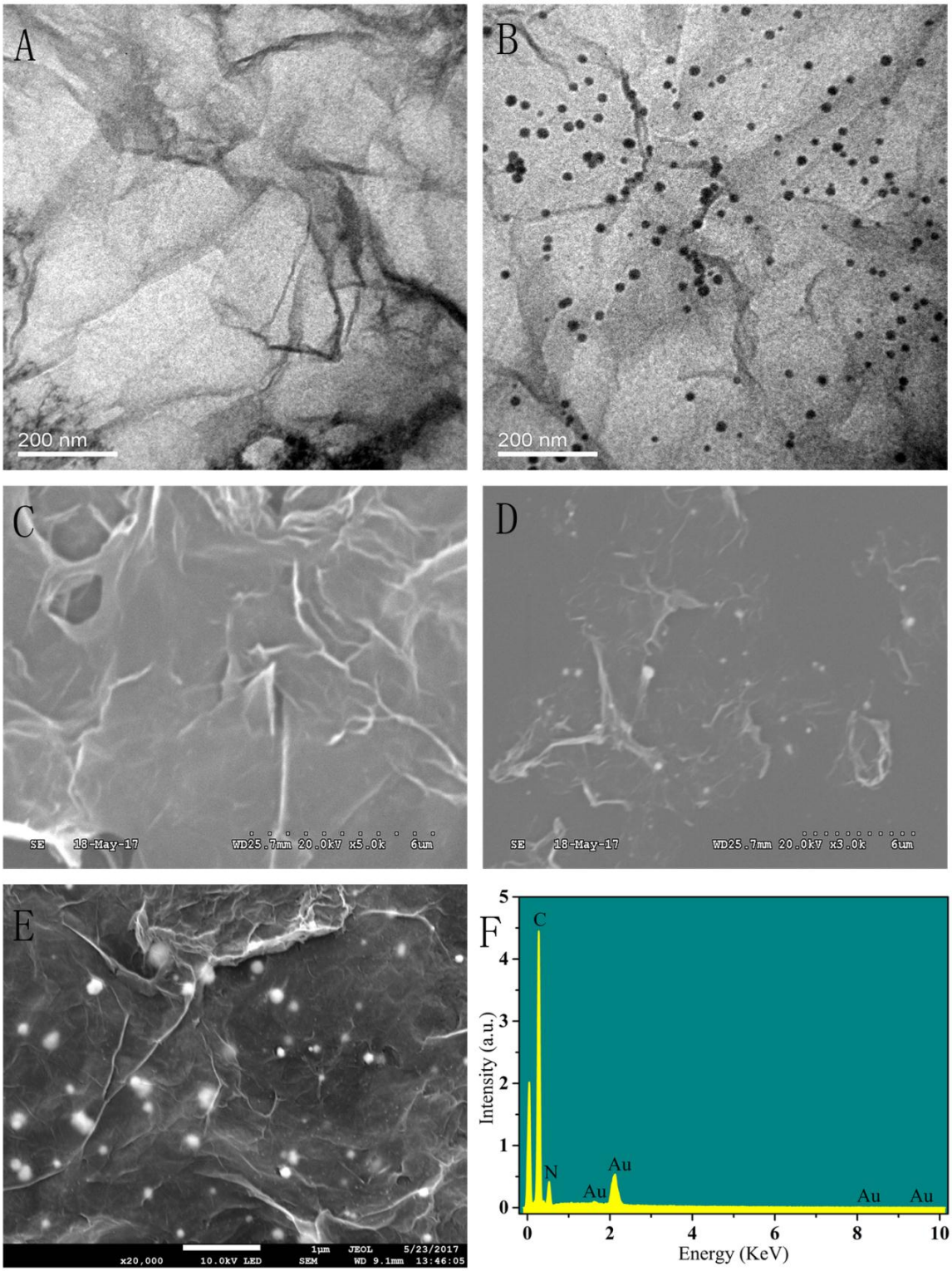

Fig. 1. (A, B) TEM images of N-G and AuNPs@N-G. (C, D) TEM images of N-G and AuNPs@N-G. FESEM image (E) and the EDS spectrum (F) of AuNPs@N-G.

3.2 Characterization of Fe-MIL-88NH$_2$ MOFs, PdNPs@Fe-MOFs microcrystals and tracer label composites

Typical UV-vis absorption spectra characterization was performed for the confirmation of the Fe-MIL-88NH$_2$ MOFs and tracer label composites. As shown in Fig. S2A, the presence of two characteristic absorption peaks at about 230 nm and 260 nm and a shoulder peak at 330 nm dominated the spectra of Fe-MIL-88NH$_2$ MOFs (curve a). After functionalization with PEI and PdNPs (curve b), the absorption peak at 260 nm converted to a shoulder peak with a slightly blue shift because the PdNPs had no absorption in the visible spectral range and impeded the collective oscillation of electrons. And a reversal peak was appeared at ~550 nm, which could be ascribed to the strong polarization property of PEI, suggesting that the success attachment and assembly on the surface of MOFs through physical adsorption. The positive charges of PEI had a substantial benefit for the adsorption of the negatively charged PdNPs. When immobilized with streptavidin and SPs, the characteristic absorption peaks were overlapped unfortunately (curve c and d). Given that, zeta-potential measurements were employed for the preparation process of the Fe-MIL-88NH$_2$ MOFs and tracer label composites. The average potential of Fe-MIL-88NH$_2$ MOFs solution was +18.3 mV (Fig. S2B), suggesting that some ferric iron (Fe^{3+}) was exposed on the surface of MOFs, which were consistent with the previous reports (Liu et al. 2015). When assembled with PEI in situ through physical adsorption, the functionalized MOFs (PEI@Fe-MIL-88NH$_2$ MOFs) with numerous positive charges were perfect building-block for further decorating PdNPs through electrostatic interaction. After decorating with PdNPs, the zeta-potential value changed to +28.1 mV, indicating that the effective attachment between PdNPs and Fe-MIL-88NH$_2$ MOFs through an electrostatic self-assembly process. When captured with streptavidin (Sa) via Pd-NH$_2$ covalent bonds, the zeta-potential value was significantly inverted to +3.2 mV, indicating the effective immobilization of Sa. After the interaction between Sa and biotin, the biotin-labeled nucleic acid probes were grafted onto the surface of MOFs and the tracer labels were fabricated successfully.

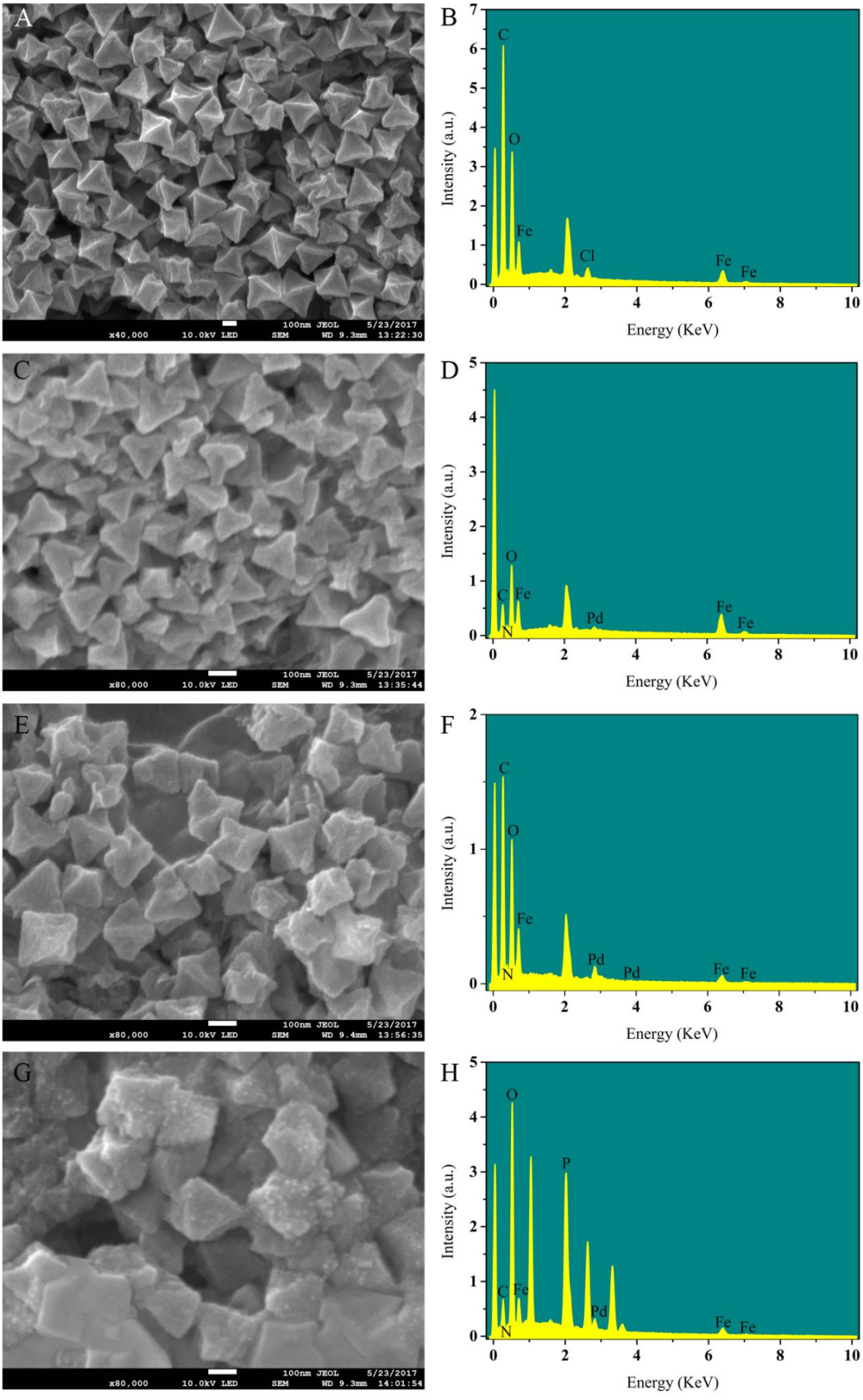
A
x40,000 10.0kV LED 100nm JEOL SEM 5/23/2017 WD 9.3mm 13:22:30
B
C
O
Fe
Cl
Fe
Fe
Intensity (a.u.)
Energy (KeV)
C
x80,000 10.0kV LED 100nm JEOL SEM 5/23/2017 WD 9.3mm 13:35:44
D
O
C
Fe
N
Pd
Fe
Fe
Intensity (a.u.)
Energy (KeV)
E
x80,000 10.0kV LED 100nm JEOL SEM 5/23/2017 WD 9.4mm 13:56:35
F
C
O
Fe
N
Pd
Pd
Fe
Fe
Intensity (a.u.)
Energy (KeV)
G
x80,000 10.0kV LED 100nm JEOL SEM 5/23/2017 WD 9.3mm 14:01:54
H
O
P
C
Fe
N
Pd
Fe
Fe
Intensity (a.u.)
Energy (KeV)

Fig. 2. FESEM image of Fe-MIL-88NH_2 MOFs (A), PdNPs@Fe-MOFs (C), Sa/PdNPs@Fe-MOFs (E) and the tracer label (G). The EDS spectra of Fe-MIL-88NH_2 MOFs (B), PdNPs@Fe-MOFs (D), Sa/PdNPs@Fe-MOFs (F) and the tracer label (H).

Subsequently, the morphology and size of the as-prepared nanomaterial were characterized by FESEM at an acceleration voltage of 10.0 kV. As shown in Fig. 2A, most of the Fe-MIL-88NH_2 MOFs suggested regular octahedron with an average diameter of 200 nm approximately, which was consistent with our previous reports (Chen et al. 2017). And the corresponding energy dispersive X-ray spectroscopy showed the peaks of C, O and Fe elements (Fig. 2B), further confirming the formation of Fe-MIL-88NH_2 MOFs. After PdNPs anchored onto the surface of PEI@ Fe-MIL-88NH_2 MOFs, the obtained hybrids showed a little different octahedron and capped with some tiny particles (Fig. 2C), indicating that the PdNPs and PEI were assembled successfully. Meanwhile, the characteristic peak of Pd element appeared due to the superficial decoration of PdNPs (Fig. 2D), which further demonstrated the above speculation. After covalent bound with Sa for aging treatment, the attached particles enlarged and the morphology changed irregular with a larger surface area (Fig. 2E). After the interaction between Sa and the biotin-labeled nucleic acid probes, numerous ashine particles were uniformly attached outside the surface of MOFs (Fig. 2G), and the intensive peak of P element presumably originated from nucleic acid probes was displayed (Fig. 2H), both of which confirmed the successful fabrication of tracer label.

3.3 Evaluation of peroxidase mimicking activity of PdNPs@Fe-MOFs microcrystals

After the successful fabrication of the PdNPs@Fe-MOFs microcrystals, the peroxidase-like activity was investigated by catalysis of the peroxidase substrate TMB in the presence or absence of H_2O_2 (Wang et al. 2017). As shown in Fig. S3, the control groups indicated that the alone TMB or H_2O_2 and TMB solution exhibited a negligible color change (curve a, c). Interestingly, the MOFs system (curse e) along

with TMB and H_2O_2 incubated at 37 ºC for 10 min showed a deep blue color with strong absorbance at 650 nm and 370 nm, which ascribed to the charge-transfer complexes derived from the one-electron oxidation of TMB (Ge et al. 2015). And another MOFs system (curve b) only showed a slight color change in the absence of H_2O_2, which could be attributed to the oxidase mimicking activity of MOFs. Meanwhile, these results also confirmed that the Fe-MIL-88NH_2 MOFs possessed the intrinsic oxidase mimicking activity of TMB in the presence of H_2O_2. It has been reported that PdNPs exhibited the excellent peroxidase-like activity. After decorating with PdNPs, the PdNPs@Fe-MOFs hybrids (curve f) showed a deeper color change with larger absorption peak than those of the pure MOFs or PdNPs (curve d) under the same condition. This catalytic activity amplification could be ascribed to the synergistic effect between the PdNPs and MOFs, which was beneficial for the detection of the low concentration of target.

3.4 Characterization of the biosensor

When perpendicularly immobilized and orderly oriented on the electrode surface with the nucleotide sequences sufficiently separated one from another, the maximum accessibility of CPs could be hybridized and more targets could be captured (Chiorcea Paquim et al. 2004; Shen et al. 2016). The “inserting” method that CPs inserted in the interspaces of MCH after the self-assembly of MCH onto the modified electrode could effectively regulate the spatial distribution and orientation of CPs (Josephs and Ye 2013). The suitable density of MCH could promote CPs standing and uniformly distributing onto the electrode surface. This hypothesis was tested by two comparison experiments that employed the proposed method and traditional “backfilling” method, respectively. As shown in Fig. 3A, the electron transfer resistance values of the proposed method (curve a) was larger than the traditional method (curve b), indicating that more CPs were immobilized on the electrode. Meanwhile, methylene blue (MB) as an electron mediator could be inserted into negatively charged nucleotide single and double chains, and which was proportional to the amount of CPs (Shen et al. 2016). The MB current response of the proposed method (curve a) was higher than

that of the traditional method (curve b) in Fig. 3B. These data suggested that the proposed strategy in work could improve the sensitivity of the biosensor.

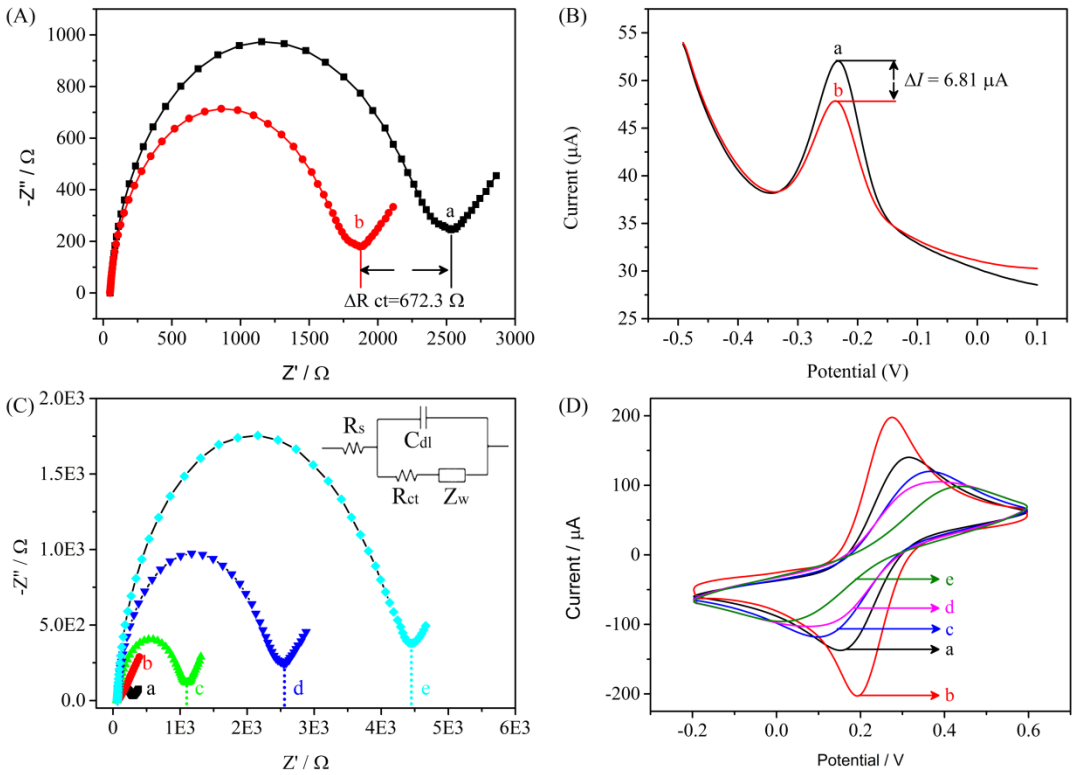

Fig. 3. EIS (A) and DPV (B) responses of different fabricated electrodes: (a) CPs were inserted in the MCH interspaces after the assembly of MCH onto the modified electrode and (b) MCH blocked after the immobilization of CPs onto the modified electrode surface. EIS (C) and CV (D) of different modified electrodes in 5 mM $[Fe(CN)_6]^{3-/4-}$ solution containing 0.1 M KCl: (a) a bare electrode, (b) AuNPs-PEI@N-G/GCE, (c) MCH/AuNPs-PEI@N-G/GCE, (d) immobilization of CPs on electrode, and (e) after incubation with 1 pM miR-122 and the tracer label 2.

EIS was employed to monitor the fabrication processes and the interface properties of the modified electrodes surface using $[Fe(CN)_6]^{3-/4-}$ as a redox probe (Bai et al. 2017; Li et al. 2015a). The Nyquist diagrams of the different modified electrodes were shown in Fig. 3C. The impedance spectra consisted of a semicircle portion and a linear portion. The linear portion at lower frequencies represented the diffusion-limited process, and the semicircle portion at higher frequencies

corresponded to the electron-transfer limited process. And the semicircle diameter of EIS was equal to the electron transfer resistance (Li et al. 2015a). A relatively electron transfer resistance with a small semicircle domain was obtained with the bare electrode (curve a). After the modification of AuNPs-PEI@N-G hybrids on the electrode surface, the resistance (curve b) decreased than that of GCE, suggesting that the AuNPs-PEI@N-G was successfully formed an interpenetrating film in favor of interfacial and redox probe electron transfer on the electrode surface. Then, the resistance (curve c) remarkably increased when non-conductive MCH was immobilized onto the modified electrode. After inserting CPs into the interspaces of MCH, the semicircle further increased (curve d) resulted from the negative charges of deoxyribose-phosphate backbones of CPs impeded the diffusion of $[Fe(CN)_6]^{3-/4-}$ toward the electrode surface (Zhao et al. 2015). As expected, the semicircle dramatically increased (curve e) after incubating with the target (1 pM miR-122) and the tracer indicators 1 (1 mg mL^{-1}) for 75 min, which was attributed to the electrostatic repulsion and the steric hindrance of the tracer bioconjugates. The inset in Fig. 3C (top right corner) was the equivalent circuit employed to fit the impedance spectra. This circuit consisted of the electrolyte resistance (R_s), the charge electron transfer resistance (R_{ct}), the double-layer capacitance (C_{dl}), and the Warbury impedance (Z_w). The values of the equivalent circuit parameters obtained after fitting curves by ZSimpWin (v 3.6) software were recorded in Table S2. With layer-by-layer assembly, the impedance values and changes of the stepwise processes confirmed that the fabrication of biosensor was successful. Simultaneously, CV was used for monitoring the stepwise fabrication processes and the resulting voltammograms were shown in Fig. 3D. The experiment results were in accordance with EIS measurement, indicating that the successful construction of the biosensor.

3.5 Analytical performances of the biosensor for miR-122

The analytical performance of the proposed miR-122 biosensor was evaluated by EIS and amperometric measurement, respectively. Firstly, EIS was employed to investigate the performance of the label-free biosensor incubated with various

concentrations of miR-122 by using [$Fe(CN)_6^{3-/4-}$] as an electrochemical indicator under the optimal parameters. The electron transfer resistance of the proposed biosensor was straightforwardly related to the amount of nucleic acid duplexes on the electrode surface because the negative nucleic acid backbones repelled [$Fe(CN)_6^{3-/4-}$] from approaching the electrode via the electrostatic repulsion. As shown in Fig. 4A, with increasing concentration of miR-122, R_{ct} value gradually increased which was assigned to the increasing nucleotide chains captured onto the electrode surface. The variation in R_{ct} change (vs. $R_{ct\ C=0}$) of the biosensor was proportional to the logarithm of the miR-122 concentration ranged from 10 fM to 100 nM (Fig. 4C). The linear relationship could be presented as ΔR_{ct} = 449.15*log C (fM) + 548.97. However, the direct-type biosensor showed an inferior analytical capability as the content of miR-122 below 10 fM.

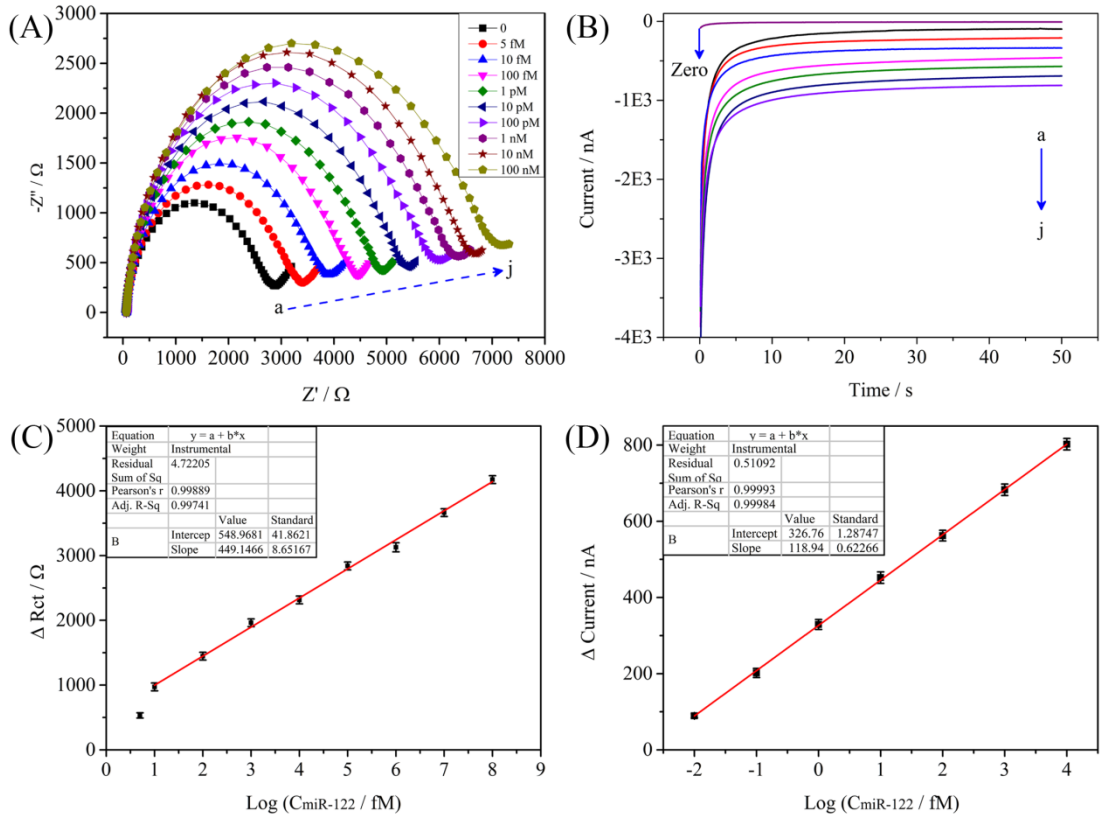

Fig. 4. EIS responses (A) and the corresponding curves (C) of the label-free biosensor incubated with different concentration of miR-122 (from a to j: 0, 5 fM, 10 fM, 100 fM, 1 pM, 10 pM, 100 pM, 1 nM, 10 nM and 100 nM) in 5 mM [$Fe(CN)_6^{3-/4-}$]. Amperometric curves (B) and the corresponding curves (D) of the proposed biosensor

incubated with different concentration of miR-122 (from a to j: 0, 0.01 fM, 0.1 fM, 100 fM, 1 fM, 10 fM, 100 fM, 1 pM and 10 pM) in 0.1 M PBS (pH 4.0) containing 1 mM TMB and 20 μM H_2O_2.

Meanwhile, the analytical performance of the proposed biosensor, a sandwich-type sensor, was investigated by amperometric measurement under the optimal conditions. As shown in Fig. 4 B, i-t current responses increased with the increasing miR-122 concentrations (curves a-j) and the linear ranged from 0.01 fM to 10 pM. And the linear relationship in Fig. 4D could be expressed as ΔI = 118.94*log C (fM) + 326.76 with a correlation coefficient of 0.9998. More importantly, the proposed biosensor had a lower detection limit of 0.003 fM (S/N=3), suggesting that it might have the superiority on tracer analysis of miR-122 in the early stage of liver injury. The excellent performance could be ascribed to the signal generation and amplification of PdNPs@Fe-MOFs mediated nonenzymatic co-reaction of TMB-H_2O_2 system and target-catalyzed hairpin assembly. In addition, the analytical performance of the proposed biosensor for miR-122 detection was compared with those previous reported (Kilic et al. 2016; Venkateswaran et al. 2016) and the results were shown in Table S3.

3.6 Analytical application of the biosensor in real sample

To assess the analytical feasibility and application of the proposed biosensor in real samples, recovery experiment was performed in the spiked serum samples by standard addition method. Subsequently, the samples were analyzed by the as-prepared biosensor and the results were recorded in Table S4. The range of variation of the recovery was from 102.5% to 106.8%, and the standard deviations were between 2.62% to 4.72% (n=5). These results suggested that the fabricated electrochemical biosensor was applicable for detection of miR-122 in real biological samples.

In view of sensitivity and specificity of the developed biosensor, the performance for miR-122 detection in healthy human serum was investigated in this work. The serum samples were provided by a blood transfusion department of southwest hospital.

The content of miR-122 was determined by the proposed biosensor and quantitative real-time polymerase chain reaction (qRT-PCR), respectively. As shown in Table 1, the results obtained from the biosensor were in good agreement with that of qRT-PCR of the same samples. More importantly, our method was less time-consuming and more facile than qRT-PCR. The proposed biosensor presented high sensitivity and speed, and showed a promising application for the direct determination of miR-122 without pretreatment in biological samples.

Table 1

Detection of miR-122 in healthy human serum with the proposed biosensor

Specimen number	qRT-PCR (fM)[a]	Proposed assay (fM)[a]
1	37.42	38.40
2	20.52	20.27
3	43.60	42.92
4	25.48	26.12
5	27.39	26.58
6	31.17	29.30
7	35.84	37.51
8	43.63	41.25
9	27.13	25.58
10	31.67	29.59

[a] Calculated as a mean of three measurements.

4. Conclusion

In summary, a new amplification strategy integrated nonenzymatic reaction with target-catalyzed hairpin assembly was constructed and applied for ultrasensitive miR-122 detection in human serum for the first time. Primarily, nonenzymatic reaction of the peroxidase substrate (TMB) in the presence of H_2O_2 was conducted by PdNPs@Fe-MOFs nanohybrids in PBS solution (pH 4.0). The nanohybrids with large surface area, numerous active sites, and fascinating catalytic activity could be served as the nanocarriers for constructing signal probes and redox probes without the addition of peroxidase or catalase, which could simplify the operation procedure and also improve the stability of catalytic activity and the proposed biosensor. As expected,

the catalytic activity and current response were enhanced by the strong bimetallic synergistic effects between PdNPs and Fe-MIL-88NH_2 MOFs. Finally, the current response and the sensitivity of the nanohybrids-assisted signal enhancement were further amplified by the target-catalyzed hairpin assembly. The developed electrochemical biosensor exhibited good sensitivity and selectivity, and was demonstrated its application for rapid and high-sensitive detection of miR-122 in real serum samples, which provided a new and innovative technology platform for rapid identification of early stage of liver injury. Moreover, our designed sensor could be applied to other microRNA through substituting for rationally probes according to the target microRNA.

Acknowledgements

The authors gratefully acknowledge the financial support of the Chongqing Municipal Engineering Technology Research Center Construction Project (CSTC2015zdcy-ztzx120005) and the Research Fund for Nursery Plan of Southwest Hospital (JCYB-179).

References

Antoine, D.J., Dear, J.W., Lewis, P.S., Platt, V., Coyle, J., Masson, M., Thanacoody, R.H., Gray, A.J., Webb, D.J., Moggs, J.G., Bateman, D.N., Goldring, C.E., Park, B.K., 2013. Hepatology 58(2), 777-787.

Bai, L., Chen, Y., Bai, Y., Chen, Y., Zhou, J., Huang, A., 2017. Biomaterials 133, 11-19.

Chen, J., Yu, C., Zhao, Y., Niu, Y., Zhang, L., Yu, Y., Wu, J., He, J., 2017. Biosens. Bioelectron. 91, 892-899.

Chen, M., Hou, C., Huo, D., Bao, J., Fa, H., Shen, C., 2016. Biosens. Bioelectron. 85, 684-691.

Chiorcea Paquim, A.M., Diculescu, V.C., Oretskaya, T.S., Oliveira Brett, A.M., 2004. Biosens. Bioelectron. 20(5), 933-944.

Fontana, R.J., Hayashi, P.H., Gu, J., Reddy, K.R., Barnhart, H., Watkins, P.B., Serrano, J., Lee, W.M., Chalasani, N., Stolz, A., Davern, T., Talwakar, J.A., Network, D., 2014. Gastroenterology 147(1), 96-108 e104.

Ge, S., Liu, W., Liu, H., Liu, F., Yu, J., Yan, M., Huang, J., 2015. Biosens. Bioelectron. 71, 456-462.

Huang, J., Zhang, L., Chen, B., Ji, N., Chen, F., Zhang, Y., Zhang, Z., 2010. Nanoscale 2(12), 2733-2738.

Huang, J., Zhu, Y., Zhong, H., Yang, X., Li, C., 2014. ACS Appl. Mater. Interfaces 6(10), 7055-7062.

Jiang, Z., Gao, P., Yang, L., Huang, C., Li, Y., 2015. Anal Chem 87(24), 12177-12182.

Josephs, E.A., Ye, T., 2013. Acs Nano. 7(4), 3653-3660.

Kilic, T., Kaplan, M., Demiroglu, S., Erdem, A., Ozsoz, M., 2016. J. Electrochem Soc. 163(6), B227-B233.

Larrey, D., Pageaux, G.P., 2005. Eur. J. Gastroenterol. Hepatol. 17(2), 141-143.

Li, Y., He, J., Niu, Y., Yu, C., 2015a. Biosens. Bioelectron. 74, 953-959.

Li, Y., He, J., Xia, C., Gao, L., Yu, C., 2015b. Biosens. Bioelectron. 70, 392-397.

Liu, M., Song, J., Shuang, S., Dong, C., Brennan, J.D., Li, Y., 2014. Acs Nano. 8(6), 5564-5573.

Liu, S., Wang, Y., Ming, J., Lin, Y., Cheng, C., Li, F., 2013. Biosens. Bioelectron. 49, 472-477.

Liu, Y.L., Fu, W.L., Li, C.M., Huang, C.Z., Li, Y.F., 2015. Anal. Chim. Acta 861, 55-61.

Mishra, S., Ghosh, S., Mukhopadhyay, R., 2014. Langmuir 30(34), 10389-10397.

Orendorff, C.J., Sau, T.K., Murphy, C.J., 2006. Small 2(5), 636-639.

Paredes, J.I., Villar-Rodil, S., Martinez-Alonso, A., Tascon, J.M., 2008. Langmuir 24(19), 10560-10564.

Shen, H., Yang, J., Chen, Z., Chen, X., Wang, L., Hu, J., Ji, F., Xie, G., Feng, W., 2016. Biosens. Bioelectron. 81, 495-502.

Shuai, H.L., Huang, K.J., Xing, L.L., Chen, Y.X., 2016. Biosens. Bioelectron. 86, 337-345.

Starkey Lewis, P.J., Dear, J., Platt, V., Simpson, K.J., Craig, D.G., Antoine, D.J., French, N.S., Dhaun, N., Webb, D.J., Costello, E.M., Neoptolemos, J.P., Moggs, J., Goldring, C.E., Park, B.K., 2011. Hepatology 54(5), 1767-1776.

Su, S., Cao, W., Liu, W., Lu, Z., Zhu, D., Chao, J., Weng, L., Wang, L., Fan, C., Wang, L., 2017. Biosens. Bioelectron. 94, 552-559.

Sun, X., Guo, S., Chung, C.S., Zhu, W., Sun, S., 2013. Adv. Mater. 25(1), 132-136.

Thomson, J.M., Parker, J., Perou, C.M., Hammond, S.M., 2004. Nat. Methods 1(1), 47-53.

Valoczi, A., Hornyik, C., Varga, N., Burgyan, J., Kauppinen, S., Havelda, Z., 2004. Nucleic Acids Res. 32(22), e175.

Venkateswaran, S., Luque-Gonzalez, M.A., Tabraue-Chavez, M., Fara, M.A., Lopez-Longarela, B., Cano-Cortes, V., Lopez-Delgado, F.J., Sanchez-Martin, R.M., Ilyine, H., Bradley, M., Pernagallo, S., Diaz-Mochon, J.J., 2016. Talanta 161, 489-496.

Wang, C., Zhou, H., Zhu, W., Li, H., Jiang, J., Shen, G., Yu, R., 2013. Biosens. Bioelectron. 47, 324-328.

Wang, X., Cao, W., Qin, L., Lin, T., Chen, W., Lin, S., Yao, J., Zhao, X., Zhou, M., Hang, C., Wei, H., 2017. Theranostics 7(8), 2277-2286.

Wang, Y., Zhu, Y., Binyam, A., Liu, M., Wu, Y., Li, F., 2016. Biosens. Bioelectron. 86, 432-438.

Wu, S., Huang, H., Feng, X., Du, C., Song, W., 2017. Talanta 167, 385-391.

Xia, N., Zhang, Y., Wei, X., Huang, Y., Liu, L., 2015. Anal. Chim. Acta 878, 95-101.

Xie, S., Ye, J., Yuan, Y., Chai, Y., Yuan, R., 2015. Nanoscale. 7(43), 18232-18238.

Yu, C.Y., Yin, B.C., Ye, B.C., 2013. Chem. Commun. 49(74), 8247-8249.

Yu, Y.Q., Wang, J.P., Zhao, M., Hong, L.R., Chai, Y.Q., Yuan, R., Zhuo, Y., 2016. Biosens. Bioelectron. 77, 442-450.

Zhang, X., Wu, D., Liu, Z., Cai, S., Zhao, Y., Chen, M., Xia, Y., Li, C., Zhang, J., Chen, J., 2014. Chem. Commun. 50(82), 12375-12377.

Zhao, M., Zhuo, Y., Chai, Y.Q., Yuan, R., 2015. Biomaterials. 52, 476-483.

Highlights:

1. A signal amplification strategy was based on target-catalyzed hairpin assembly and metal-organic frameworks (PdNPs@Fe-MOFs) mimetic enzyme co-reaction.
2. A new type of multifunctional iron based metal-organic frameworks possessed of excellent peroxidase-like activity and was designed and applied for sandwich-type biosensor for the first time.
3. It was demonstrated that “inserting” method was superior to traditional “backfilling” method for the fabrication of nucleic acid biosensor.
4. The biosensor was with a detection limit of 0.003 fM (S/N=3) and a linear range from 0.01 fM to 10 pM.
5. The biosensor was successfully used for detecting miR-122 in human serum, and provided a rapid and efficient method for detecting drug-induced liver injury at early stage.